# The impact of long-term changes in ocean waves and storm surge on coastal shoreline change: A case study of Bass Strait and south-east Australia

Mandana Ghanavati[1], Ian R. Young*[1], Ebru Kirezci[1], Jin Liu[1]

[1]Department of Infrastructure Engineering, University of Melbourne, Melbourne, VIC 3010, Australia.
* Corresponding author: ian.young@unimelb.edu.au

## Abstract

Numerous studies have demonstrated that significant global changes in wave and storm surge conditions have occurred over recent decades and are expected to continue out to at least 2100. This raises the question as to whether the observed and projected changes in waves and storm surges, will impact coastlines in the future? Previous global-scale analyses of these issues have been inconclusive. This study investigates the south-east coast of Australia over a period of 26 years (1988-2013). Over this period, this area has experienced some of the largest changes in wave climate of any coastal region, globally. The analysis uses high-resolution hindcast data of waves and storm surge, together with satellite observations of shoreline change. All datasets have been previously extensively validated against in situ measurements. The data are analysed to determine trends in each of these quantities over this period. The coastline is partitioned into regions and spatial consistency between trends in each of the quantities investigated. The results show that beaches along this region appear to have responded to the increases in wave energy flux and changes in wave direction. This has enhanced non-equilibrium longshore drift. Long sections of the coastline show small but measurable recession before sediment transported along the coast is intercepted by prominent headlands. The recession is largest where there are strong trends of increasing wave energy flux and/or changes in wave direction, with recession rates of up to 1m/year. Although a regional study, this finding has global implications for shoreline stability in a changing climate.

## 1. Introduction

Sandy coastlines are dynamic systems, responding to changes in waves, storm surge, sea level, available coastal sediment supply and human activities (e.g. coastal structures, beach nourishment) (Komar, 1998; Masselink, et al., 2016). These changes occur on a variety of spatial and temporal scales. Spatially, changes in beach alignment and the presence of coastal shoreline features (headlands and bays) impact both the wave climate for individual beaches and the characteristics of longshore drift. At temporal scales of days, beach erosion results from individual storms (Komar, 1998; Harley, et al., 2017; Masselink, et al., 2016). At time scales of 2 to 10 years, changes in storminess associated with climate indices (e.g. El Niño) (Ranasinghe, et al., 2004; Harley, et al., 2011; Barnard, et al., 2015; Vos, et al., 2023) can result in sustained impacts on beach systems. Longer term changes in mean sea level as a result of climate change are also predicted to result in coastal recession (Hinkel, et al., 2013; Ranasinghe, 2016; Vousdoukas, et al., 2020; Ranasinghe, et al., 2021; Vitousek, et al., 2023). It should be noted that throughout this paper

we refer to shorter-term changes in beach location due to storms or a series of storms as erosion or accretion. Longer-term changes such as those due to climate change are referred to as recession or progradation.

Waves and storm surges are generated by environmental variables (wind and sea level pressure gradient). It has been shown that these environmental variables are impacted by climate change and hence long-term historical changes (trends) in waves (Wang & Swail, 2001; Wang, et al., 2009; Hemer, 2010; Young, et al., 2011; Aydoğan & Ayat, 2018; Zheng & Li, 2017; Young & Ribal, 2019; Takbash & Young, 2020; Reguero, et al., 2019; Cao, et al., 2021) (Young & Ribal, 2022; Liu, et al., 2022; Morim, et al., 2022; Erikson, et al., 2022) and storm surges (Paprotny, 2014; Androulidakis, et al., 2015; Cid, et al., 2016; Muis, et al., 2016; Kim, et al., 2017; Feng, et al., 2018; Ghanavati, et al., 2023) have been observed. A number of studies have also projected continued global increases (positive trends) in wave height over the 21st century, particularly in the Southern Hemisphere, under plausible climate change scenarios (Hemer, et al., 2013; Meucci, et al., 2020; Hochet, et al., 2021; Liu, et al., 2022; Meucci, et al., 2023; Morim, et al., 2023; Liu, et al., 2023).

If sandy coasts are impacted by changes in wave and storm surge conditions, the potential for continued increases in the values of these variables in the future raises the question as to what impact this may have on sandy coastlines and associated communities. As a means of determining potential future impacts, the obvious precursor is to assess the impacts that historical changes in long-term wave and storm surge conditions have had on coastlines. In the first study of its type, Ghanavati, et al. (2023) investigated this issue at global scale by using long-term modelled wave and storm surge data together with satellite observations of beach recession/progradation over the last 30 years. They found that, noting the relatively small trends in wave and storm surge conditions over this period, the accuracy of the available data, and other unrelated impacts on shoreline response (e.g. availability of sediment, human impacts), no clear relationship was evident.

In order to adress the limitation of the Ghanavati, et al (2023) work, the present study examines, in much finer detail, the south-east coastline of Australia. This is an area where long-term trends in wave conditions are some of the largest in the world, responding to changes in wave climate in the Southern Ocean (Liu, et al., 2022). Therefore, if there is a causal link between changes in long-term wave and storm surge climate and shoreline response, one would expect clear signs in this region. As a regional area is considered, it is possible to use higher resolution data (both model and satellite) removing uncertainties in the global-scale Ghanavati, et al (2023) study. In addition, the regional-scale study enables an analysis of the role beach compartments play in defining sediment transport. As such, one can investigate changes in longshore drift due to changes in wave climate and the characteristic signature of such non-equilibrium transport with eroding beaches and deposition of sediment behind peninsulas.

Although the present study is regional, the area being studied is a proxy for the potential impacts one may see in other regions of the world as changes in wave and storm surge climate are projected

to continue to change in the future. Hence, the findings of the study have global implications for shoreline response in the future. The study is unique in that it has been possible to combine high resolution datasets for waves, storm surge and shoreline response and addresses a previously unexplored area of shoreline response in a changing climate.

The structure of the paper is as follows. Section 2 outlines the study area, data sets and analysis techniques used in the study. Results are given in Section 3, including the observed relationships between changes in wave and storm surge quantities and beach recession/progradation. Discussion and conclusions are provided in Section 4.

## 2. Methodology

### *2.1 Study Area*

The study region is shown in Figures 1 and 2, and covers an area of 137E°–155°E, 35S°–45°S. Three Australian coastal states span this domain, Victoria, southern New South Wales and the island of Tasmania in the south of the domain. The south-eastern coast of the mainland of Australia (Victoria), the coastal area of the study, is separated from Tasmania by the relatively shallow Bass Strait. The area is exposed to a particularly complex wave climate (Liu, et al., 2022). To the west, the coast is exposed to the Southern Ocean and hence experiences a very energetic wave climate with recorded significant wave height as high as 10m (Meucci, et al., 2023). The wave climate of this region is dominated by south-westerly Southern Ocean swell. Central regions of the study domain are protected by the island of Tasmania and have a mixed wave climate with swell from both the south-west and south-east and locally generated wind sea. To the east, the wave climate is more heavily dependent on the local wind-sea but with south-easterly swell still playing a role (Liu, et al., 2022).

Both observational data from satellite altimeters (Young, et al., 2011; Young & Ribal, 2019; Timmermans, et al., 2020) and model hindcasts (and reanalyzes) (Cao, et al., 2021; Young & Ribal, 2022) show that over the last 35 years, there has been a small global increase in mean significant wave height. This increase is largest in the Southern Ocean (approximately 3mm/year or an increase of 3% over the last 30 years), which results in impacts across the Indian, South Pacific and South Atlantic Oceans due to radiating swell. Therefore, the study area is a location where relatively large changes in significant wave height have occurred over the period.

### *2.2 Datasets*

This study uses regional datasets for each of wave, storm surge, and coastal change from which the historical trend magnitudes of the various quantities were calculated. The datasets under consideration cover different periods of time, and thus, to ensure consistency across analyses, a

common time period from 1988 to 2013 was selected. A description of each dataset used in the study is provided below.

*Liu et al. (2022) regional wave hindcast* is a high-resolution regional wave hindcast dataset based on a WAVEWATCH III model with an ST6 physics package (Liu, et al., 2021). The regional model covers the domain shown in Figure 2 using an unstructured grid with a coastal resolution as small as 500m and a coarser deep water resolution as large as 10km. The regional model is nested within a global model using the same ST6 physics (Liu, et al., 2021). Both the regional and global models are forced with ERA5 winds (Hersbach, et al., 2020). The regional wave model dataset has been extensively validated (Liu, et al., 2022; Liu, et al., 2023) against both a network of coastal buoys and satellite altimeter data. Wave data were available from the hindcast with a temporal resolution of 1 hour. The period of the hindcast was from 1981 to 2020. The dataset's high resolution is particularly important for studying coastal regions, where wave conditions can vary significantly over short distances. Additionally, the long period of coverage allows us to identify and analyze trends in the wave climate over several decades, providing insight into the possible effects of historical climate change on the region.

*Colberg, et al. (2018) Australian water level hindcast* is a dataset of sea level simulations for the Australian coastline. The dataset was generated using the Regional Ocean Modelling System (ROMS) (Shchepetkin & McWilliams, 2005), which was run in a depth-integrated form on a 5 km resolution grid for the Australian region. Tidal currents and heights at open boundaries were specified from the TPXO7.2 global model (Egbert & Erofeeva, 2002). TPXO7.2 best fits (in a least squares sense) the Laplace tidal equations and along track averaged data from TOPEX/Poseidon and Jason altimetry data. The ROMS model was run for the period 1981-2013 and was forced with NCEP Climate Forecast System Reanalysis (CFSR) (Saha, et al., 2010) wind and surface pressure data. The model has been validated at 14 tide gauge locations around the Australian coastline (Colberg, et al., 2018). Again, the output was available on an hourly basis.

*Bishop-Taylor et al., (2021) Geoscience Australia beach dataset* is a high-resolution regional dataset of shoreline change rate for the coast of Australia. The dataset utilizes a combination of satellite visual data and tidal modelling to map shoreline change, with an along-coast resolution of 30m for non-rocky (sandy or muddy) areas. The dataset provides annual values of the shoreline position over the period 1988 to 2019. The dataset has been extensively validated using in-situ measurements, comprising 330 validation transects, each spanning over 10 years of coastal monitoring data. The Mean Absolute Error (MAE) in the trend across these validation points was 0.35 m/year (Bishop-Taylor, et al., 2021).

### *2.3 Trend calculation*

Each of the datasets (waves, storm surge, shoreline location) are defined at different resolution and in different manners (structured and unstructured grids, specific shoreline positions), therefore none of these quantities are co-located. As shown by Ghanavati, et al., (2023) and subsequently

confirmed in Figures 3, 4 and 5, trends in both wave height and storm surge quantities generally vary smoothly along extended coastal regions (100s of kilometres). Shoreline recession/progradation rate can, however, vary rapidly in magnitude and sign over relatively short spatial scales (10s of kilometres) (Luijendijk, et al., 2018; Ghanavati, et al., 2023). That is, one beach can be receding whilst the next is prograding. As such, simple scatter plots of rates of change of wave and storm surge quantities verses recession/pogradation rates are not meaningful. Rather, one needs to consider relationships over spatial regions of the coastline. To achieve such an analysis, we divide the study domain in Figure 1 into six regions, each spanning 2° in longitude – (a) 138E°-140E°, (b) 140E°-142E°, (c) 142E°-144E°, (d) 144E°-146E°, (e) 146E°-148E° and (f) 148E°-150E° from west to east. These regions span the differing wave climates of the study domain (see Figure 2 and subsequent discussion). For analysis purposes, we present data as follows. Wave quantities are presented both as colour shaded plots, and at shoreline locations corresponding to ocean points defined by the unstructured WAVEWATCH III computational grid. Storm surge quantities are shown at the locations corresponding to the ocean points nearest the land/sea transition of the ROMS 5km computational grid. Coastal change points are as defined at coastal locations in the Bishop-Taylor et al., (2021) dataset, which has an along-cost resolution of 30m.

Each of the three datasets used in the study covers a different period of time: wave hindcast - 1981 to 2020, storm surge data - 1981 to 2013, and shoreline change data - 1988 to 2019. To ensure a consistent evaluation of the trends and variability in the oceanic parameters, a common analysis period of 1988 to 2013 was selected for the study.

For each of the datasets, a range of quantities to be investigated were calculated. These include: waves – mean significant wave height ($H_s$), 95$^{th}$ percentile significant wave height ($H_s^{95}$), mean wave energy flux ($C_g E$), mean wave period ($T_m$) and mean wave direction ($\theta_m$), where $C_g$ is the group velocity of waves and $E = H_s^2/16$ is the wave energy. The hourly data from the regional wave model was used to calculate annual values of each of these quantities.

As noted above, various datasets have different temporal and spatial resolutions and hence slightly different approaches were used to evaluate the variability and extremes of oceanic parameters. The wave and surge time series were collected at a temporal resolution of 1 hour, while the shoreline dataset provided annual shoreline change with reference to the shoreline location in 2019. Therefore, annual mean values of wave parameters including significant wave height, wave energy flux, wave direction and wave period were calculated. Furthermore, the extremes were determined by calculating annual higher percentiles (95th, 98th, and 99th) for significant wave height and surge level. These metrics provide a consistent basis for evaluating the variability and extremes of the oceanic parameters across different datasets. As the various percentile thresholds gave similar results, extreme events were determined as occasions on which the time series exceeded the 95$^{th}$ percentile but with such events separated by a minimum of 48 hours. The number of such events

in each year were defined as $N_{H_s^{95}}$. In a similar fashion, storm surges were defined as occasions when the water surface elevation, $\eta$, exceeded the 95th percentile ($\eta^{95}$) and the number of such events was defined as $N_{\eta^{95}}$. Again, annual values of these quantities were determined. The annual values of shoreline position from the Bishop-Taylor et al. (2021) data were defined in a similar manner and represented as $C_{GA}$.

The annual values of each quantity were then used to determine linear trends over the period 1988-2013. Both linear regression and the non-parametric Tiel-Sen estimator (Sen, 1968) were used for this purpose. As the resulting values were very similar, the Sen slope estimates are used in the subsequent analysis. The resulting trend values are represented as: $\Delta H_s$, $\Delta H_s^{95}$, $\Delta C_g E$, $\Delta \theta_m$, $\Delta N_{H_s^{95}}$; $\Delta \eta^{95}$, $\Delta N_{\eta^{95}}$; $\Delta C_{GA}$.

## 3. Results

### *3.1 Wave climate*

Figure 2 shows the mean wave climate of the study area and how it has changed over the period 1988 to 2013 as indicated by the Liu, et al. (2022) hindcast. Figures 2a and 2b show the mean significant wave height $\bar{H}_s$ and wave energy flux, $\overline{C_g E} = \rho g^2 H_s^2 T_m / (64\pi)$, respectively. As noted above, the significant wave height and wave energy flux vary significantly across the study area. In the west, the coastline is exposed to energetic Southern Ocean swell with mean $H_s$ of approximately 3m. In the eastern regions of the study area, where there is protection provided by the island of Tasmania, mean $H_s$ decreases significantly to less than 1.5m, a decrease by a factor of approximately 2. The wave energy flux shows an even more significant change, with mean values varying from approximately 60kW/m in the west to 15kW/m in the east, a factor of 4. The substantial reduction in wave energy flux is attributed to the protection provided by the island of Tasmania, which leads to a decrease in both $H_s$ and $T_m$. As shown by Liu, et al. (2022), the mean/peak wave direction also changes significantly across the domain. In the west, the dominat wave direction is defined by energetic south-westerly swell. In the east, the protection provided by the island of Tasmania means that swell entering the area is predominately from the south-east.

The changes in wave climate over the study period are also significant across this region. As noted above, a range of studies have shown that the Southern Ocean wave climate has increased over the past 35 years (Young, et al., 2011; Young & Ribal, 2019; Cao, et al., 2021; Young & Ribal, 2022). Swell from the Southern Ocean dominates the western areas of the study region and hence there have been significant changes in the wave climate, as shown by Figures 2c-h. In the west, $H_s$ has increased by approximately 5% (Figure 2c) over the study period and $C_g E$ by approximately 14% (Figure 2d). In contrast, in the east, where the wave climate is not as exposed to Southern Ocean swell, these values decrease to approximately zero (no change). Figures 2e and f clearly show that

the positive trends in $H_s$ are due to changes in both swell and local wind-waves. Figure 2g also shows that there have been only small changes in $T_m$ across the domain.

The most dramatic changes in wave climate concern the mean wave direction, $\theta_m$. Over the western regions of the study domain, there has been a small counter-clockwise rotation of the mean wave direction (less than 1.5°). This is a result of the gradual southward movement of Southern Ocean low pressure systems over recent decades (Morim, et al., 2022). This small change in deep water wave direction, significantly impacts the shadow region in the lee of Tasmania and hence the wave direction, resulting in much larger counter-clockwise rotations of approximately 5° (Figure 2h). These values reduce towards the coast of mainland Australia (eastern area of study region) but are still larger than 3°.

### *3.2 Storm Surge Climate*

As noted above, storm surges were defined as events where the water surface elevation exceeded the 95$^{th}$ percentile value, $\eta^{95}$. Figure 3 and 4 show plots for each of the sub-regions referenced in Figure 1. These figures show colour contoured values of $\Delta C_g E$ (Figure 3) and $\Delta\theta_m$ (Figure 4), coastal values of $\Delta\eta^{95}$ and $\Delta C_{GA}$. In contrast to the wave climate, changes in storm surge, $\Delta\eta^{95}$ are very consistent along the coastline of the study area. Values of $\Delta\eta^{95}$ are negative along the entire coastline, decreasing in magnitude from approximately -0.3cm/year in the west to -0.2cm/year in the east. The fact that the magnitude of storm surges has been decreasing over this period is consistent with the observations of Liu, et al. (2023) that as Southern Ocean low pressure systems move south, they increase the mean atmospheric pressure and reduce the pressure gradiant over southern Australia. As surface pressure (and wind) drives storm surge, this results in a tendancy for a reduction in the magnitude of storm surges.

### *3.3 Relationship between waves, storm surge and shoreline change*

As previously shown at global scale by Luijendijk, et al. (2018) and Ghanavati, et al. (2023), recession/progradation rates vary in magnitude and sign on relatively small spatial scales. This is because sediment transport can be both offshore/onshore as well as longshore. In the case of non-equilibrium longshore transport of sediment, one would expect some beaches to recede whilst other receive sediment from these beaches and hence prograde. Ghanavati, et al. (2023) speculated that coastlines which show such non-equilibrium behaviour may be responding to long-term changes in the environmental forcing provided by trends in waves and storm surge. A causal relationship is, however, complicated by other variables which may have a larger impact on beach position. These additional factors include the availability of sediment supplied to beach compartments from fluvial sources and the impacts of human-induced interventions such as coastal structures and beach nourishment (Ranasinghe, 2016). Ghanavati, et al. (2023) limited

recession/progradation data to values in the range $\pm 1$m/year to confine the datasets to changes which may be a result of long-term processes rather than fluvial and human-induced influences, which tend to be much larger in magnitude (Luijendijk, et al., 2018).

Therefore, following these precidents, in Figures 3 – 6, the quantity $\Delta C_{GA}$ has been filtered to retain only values in the range $\pm 1$m/year. Figure 5 shows values of $\Delta C_{GA}$ (in the range $\pm 1$m/year) as a bar chart along the coastline from 138E° to 150E°. Each of the 2° regions shown in Figures 1, 4 and 5 is marked along the longitude axis. As expected, values of $\Delta C_{GA}$ in Figures 3, 4 and 5 show both positive (progradation) and negative (recession) values. To quantify recession/progradation, values of $\Delta C_{GA}$ in the range -0.05m/year to -1.00m/year are clasified as recession, values in the range +0.05m/year to +1.00m/year as progradation and values in the range $\pm$ 0.05m/year as representing stable coastlines. Table 1 shows the percentage of coastal locations classified as receding, prograding or stable under these criteria. In addition, Figure 6 shows histograms of the distribution of the magnitudes of the values of $\Delta C_{GA}$.

Table 1 and Figure 6 show that the sections (c) 142E°-144E° and (f) 148E°-150E° are predominately receding. Segment (d) 144E°-146E° shows quite large values of both recession and progradation (see Figure 5) but with more locations prograding than receding. However, this region is complicated by the presence of Port Phillip Bay. The other segements (a), (b) and (e) show no clear difference between the percentage of receding and prograding locations.

To understand the results shown in Table 1, we consider each of the two degree sections shown in Figures 3, 4 and 5. In these figures, values of the trend in wave energy flux, $\Delta C_g E$ (Figure 3) or wave direction, $\Delta \theta_m$ (Figure 4) are shown as colour shaded contours over the regions. The trend in storm surge (always negative) are shown as colour coded squares at 5km intervals along the shoreline, at the resolution of the water level model. The satellite-derived values of trend in shoreline location at each beach location (Bishop-Taylor, et al., 2021) are shown as colour coded filled circles, at the 30m along-coast resolution.

Figures 3a and 4a show the region from 138E° to 140E° (segment (a), Victor Harbour to Cape Jaffa). This region shows relatively small positive values of $\Delta C_g E$ (approximately 0.01kWm$^{-1}$/year) and a small counter-clockwise rotation of the mean wave direct (approximately -0.02deg/year or 0.6° over 30 years). In response to these small changes in wave properties there is no consistent changes in shoreline. In the western regions (138.6E°-139.2E°) the shoreline is prograding. However, this may be associated with fluvial sediments, as this region is the ocean entrance of Lake Alexandrina and the mouth of the Murray River. These results are consistent with the bar chart of Figure 5 and the results in Table 1 and Figure 6a that there is no clear difference between recession and progradation for segment (a).

Moving east to segment (b), values of $\Delta C_g E$ increase (Figure 3b) and the region shows small receding shorelines (139.6E°- 141.0E°). This changes to progradation between 141.0E°-141.2E°, west of Cape Bridgewater. This behaviour is consistent with sediment being moved along the shoreline west to east from 139.6E°- 141E° by the increasing wave energy flux and the prevailing wave direction from the south-west. This sediment transport is interrupted by Cape Bridgewater resulting in the progradation between 140.8E°-141.2E°. The overall balance between these regions results in no clear difference between locations receding and prograding in Table 1 and Figure 6b.

The strong positive trend in wave energy flux is maintained east of Cape Bridgewater (segment (c), Figures 3c) with small counter-clockwise rotation of the mean wave direction (Figure 4c). Along this extended region of the coast to Cape Otway (141.6E°-143.6E°), the coastline shows small recession (approximately -0.1m/year – 3m over the measurement period of 30 years). East of Cape Otway, the magnitude of the recession decreases and the shoreline shows little net change in location. This behaviour is consistent with the reduced impact of south-westerly swell east of Cape Otway, which provides some shelter from such waves. Table 1 and Figure 6c show that summed across the full segment (c), a total of 53% of locations are receding and only 27% prograding.

East of Cape Otway, the wave energy flux climate near the coast decreases (Figure 2b), as Cape Otway provides protection from the south-westerly swell and $\Delta C_g E$ also decreases as the protection provided by Tasmania becomes important (Figure 3d). The shoreline trends, $\Delta C_{GA}$, are complicated by the presence of Port Phillip Bay (Figures 3d, 4d). From Cape Otway to Inverloch (143.6E°- 145.8E°) there is relatively little change in $\Delta C_{GA}$. The relatively small region from Inverloch to Wilson's Promontory (145.8E° - 146.4E°) shows a receding shoreline, previously noted in studies of the area (Leach, et al., 2023). As a result, there is no clear overall differences between recession and progradation for this section (Table 1 and Figure 6d). However, if one considers just the ocean beaches (exclude Port Phillip Bay in Figures 3d and 4d), then there is small recession along the entire coastline of section (d).

East of Wilson's Promontory the coastline is characterized by very long beaches and barrier islands (Ninety-mile beach). This region from 147E° to 149.6E° (Wilson's Promontory to Cape Howe) (Figures 3e-f, 4e-f) is characterized by a large counter-clockwise rotation of the mean wave direction. The region immediately east of Wilson's Promontory (146.5°E – 147°E) shows strong progradation. The remainder of this extended coastline, however, shows consistent recession of approximately -0.5m/year (15m over the measurement period), particularly for section (f). This section shows the strongest recession of any extended section, with Table 1 showing 60% of locations receding and only 30% prograding. As noted above, the dominant swell in this region is from the south-east and, although the changes in wave energy flux are small, there has been a significant counter-clockwise rotation of the wave direction over the study period. This results in the wave direction gradually becoming more shore-parallel. Therefore, the shoreline change noted above is consistent with an increase in longshore drift (east to west) with sediment being

accumulated to the east of Wilson's Promontory. We should also note that this area east of Wilson Promontory is one of the few estuarine environments along the entire Victorian coast and hence some of the observed progradation may be due to fluvial deposits and ebb-tide delta formation (Konlechner, et al., 2020).

The results above use the percentage of coastal locations prograding or receding as the measure of whether the beach is responding to long term changes in waves and/or storm surge. As such, it does not consider the magnitudes of the progradation or recession. Figure 6 shows histograms of the magnitudes of the progradation/recession rates for each coastal sections. The figure confirms the results above showing sections (c) 142E° – 144E° and (f) 148E° – 150E° are clearly receding with other sections less clear, as explained for each section above.

In the above analysis, we speculate that changes in wave energy flux, $\Delta C_g E$ and mean wave direction, $\Delta\theta$ are the primary drivers of the observed changes in shoreline. The observed data supports this speculation. The Supplementary Material shows plots similar to Figures 3 and 4 for changes in the other related quantities: significant wave height, $\Delta H_s$ (Figures S1 a-c and S1 d-f), extreme significant wave height, $\Delta H_s^{95}$ (Figures S2 a-c and S2 d-f), mean wave period, $\Delta T_m$ (Figures S3 a-c and S3 d-f) and number of extreme wave events, $\Delta N_{H_s^{95}}$ (Figures S4 a-c and S4 d-f).

## 4. Discussion, conclusions and future work

Ghanavati, et al. (2023) found that at global scale, they could not distinguish a clear relationhip between modelled (and observed) changes in wave energy flux and storm surge over the last 30 years and changes in shoreline postion. The present dataset extends this result by considering the region of south-east Australia. This region is important in that it is an area with major spatial variations in wave energy flux climate (mean conditions) and some of the largest coastal trends in wave energy flux and mean wave direction globally in the last 30 years. In addition, both high resolution coastal wave and storm surge hindcasts are available, as well as high resolution observations of shoreline change. As such, this is a unique region to determine if observable changes in shoreline position are evident as a consequence of long term changes in wave (and/or storm surge) climate.

The results show clear changes in shoreline position, which are consistent with postive trends in wave energy flux and changes in mean wave direction. In the western regions of the domain the mean wave direction is from the south-west and there have been positive trends in wave energy flux, $\Delta C_g E$ of approximately 14% (6/43kW/m). This appears to have resulted in non-stationary longshore drift from west to east and shoreline changes of approximately 3m over the 30 year study period.

In the central regions of the study domain both the mean wave energy flux and trends in wave energy flux decrease, as the island of Tasmania provides protection from the south-westerly swell. In this region there are no consistent trends in shoreline position with a similar number of coastal locations receding and prograding. Although ocean beaches do show small recession.

To the eastern end of the study domain, the protection provided by Tasmania and the deepwater conter-clockwise rotation of the mean wave climate means that the wave shadow of Tasmania results in a relatively large counter-clockwise rotation of the mean wave direction (up to 6° over the last 30 years). These changes in mean wave direction appear to be driving non-stationary behaviour of the beach systems in the region with the coastline from 146° to 149° (approximately 300 km) receding by up to 30m over the 30 year study period.

The results presented in this analysis are consistent with a study of this same region by Konlechner, et al. (2020) using lower resolution shoreline change data (Luijendijk, et al., 2018). The shoreline change "hot-spots" of that study are consistent with the present results. The results of the present study are also consistent with the global findings of Ghanavati, et al. (2023). Here, we find that long term changes in wave climate can apparently drive long-term changes in beach location but that relatively large changes in wave energy flux and/or direction are required to produce measurable changes in beach position. As noted, the study region has both a very energetic wave climate and some of the largest trends in this climate of any coastline. However, even in a region such as this, where long-term changes in wave energy flux are relatively large, the resulting changes in beach location are only approximately 1.0 m/year or 30m over the study period.

In the present analysis, we speculate that the observed changes in shoreline position in the western section of the domain are driven by non-stationary longshore drift from west to east with sediment transport being intercepted by Cape Bridgewater. Such behaviour is consistent with the observed increases in wave energy flux and the predominately south-westerly swell. In the eastern sections of the domain, we speculate that there is sediment transport from the east to west, intercepted by Wilson's Promontory. This speculation is consistent with the predominately south-easterly swell in the region and the observed couter-clockwise change in mean wave direction over the study period.

Although such speculation is consistent with the datasets, other processes may also have an impact on shoreline change. The most obvious such change is sea level rise, which could be expected to cause shoreline recession. Observations (Watson, et al., 2015; Nerem, et al., 2018) indicate that in recent years sea level rise in the Australia region has been approximately 3mm/year. The bed slope along the south-eastern coast of Australia is on avaerage approximately 1:100 (Athanasiou, et al., 2019). Therefore, application of Bruun's rule (Bruun, 1962) would suggest a uniform recession of approximately 0.3 m/year. Such a value is smaller than, but comparable, to the observed recession in the western and eastern portions of the study domain. Recession due to sea level rise, however, would not account for the observed progradation west of Cape Bridgewater or east of Wilson's Promontory. In addition, Bishop-Taylor, et al. (2021) indicate that over their full dataset for

Australia, approximately the same number of beaches are receding (11.1%) as prograding (11.0%). Table 1 indicates that for the present study region this is also the case. Sea level rise would be expected to result in a net recession of beaches. In contrast non-equilibrium longshore drift driven by changes in wave climate will cause some beaches to recede whilst other prograde.

Therefore, we conclude that the present results are more consist with the impacts of changes in wave climate rather than sea level rise.

Although the present study is regional, it has global implications for the magnitude of changes in shoreline response which may result in other regions of the world under future projections of changes in wave climate. The present study clearly shows that impacts of changing wave climate will have strong regional characteristics and that it is important to consider the unique nature of each region in determining potential impacts. The response to individual coastal compartments will differ in terms of the magnitude of the response and even the sign (recession verses progradation).

As noted, the present analysis provides the first evidence of a causal relationship between long-term climate trends in waves and shoreline change. It does, however, have a number of limitations which should be addressed in future research if a comprehensive understanding of the impacts future projected changes in wave climate may have on our coastlines. These future studies could include:

- Detailed sediment transport modelling to assess whether the observed changes in wave energy flux and wave direction would be expected to result in non-stationary longshore drift of the magnitude observed in the recorded shoreline position.

- The extraction of shoreline position from relatively low-resolution satellite images is computationally challenging. The Bishop-Taylor, et al. (2021) dataset represents a significant advance in resoltion and accuracy. Further developments in the use of Artificial Intelligence approaches to determining shoreline postion are expected to further reduce errors in such data.

- The present analysis is limited to south-east Australia as there were opportunistic high-resolution datasets of long-term changes in waves, storm-surge and shoreline position available. Dedicated projects modelling specific areas for the purpose of better determining the relationships between changes in these quantities would better quantify the likely impacts of future changes on vulnerable shoreline.

## Code/Data availability

All data used in the paper and codes for the analysis are available from the authors upon request.

## Competing Interests

The authors declare no competing interests.

## Author Contributions

MG: Data curation, Investigation, Writing – original draft, Writing – review and editing; IY: Conceptualization, Investigation, Supervision, Writing – original draft, Writing – review and editing; EK: Writing – review and editing; JL: Writing – review and editing

## References


Androulidakis, Y. S. et al., 2015. Storm surges in the Mediterranean Sea: variability and trends under future climatic conditions. *Dynamics of Atmospheres and Oceans,* Volume 71, pp. 56-82.

Athanasiou, P. et al., 2019. Global distribution of nearshore slopes with implications for coastal retreat. *Earth System Science Data,* Volume doi.org/10.5194/essd-2019-71.

Aydoğan, B. & Ayat, B., 2018. Spatial variability of long-term trends of significant wave heights in the Black Sea. *Applied Ocean Research,* Volume 79, pp. 20-35.

Barnard, P. et al., 2015. Coastal vulnerability across the Pacific dominated by El Niño/Southern Oscillation. *Nature Geosciences,* Volume 8, p. 801–807.

Bishop-Taylor, R., Nanson, R., Sagar, S. & Lymburner, L., 2021. Mapping Australia's dynamic coastline at mean sea level using three decades of Landsat imagery. *Remote Sens. Environ.,* Volume 267, p. 112734.

Bruun, P., 1962. Sea-Level Rise as a Cause of Shore Erosion. *Proc. American Society of Civil Engineers.*

Cao, Y., Dong, C., Young, I. & Yang, Y., 2021. Global wave height slowdown trend during a recent global warming slowdown. *Remote Sensing,* Volume 13, p. 4096.

Cid, A. et al., 2016. Long-term changes in the frequency, intensity and duration of extreme storm surge events in southern Europe.. *Climate Dynamics,* 46(5), p. 1503–1516.

Colberg, F., McInnes, K., O'Grady, J. & Hoeke, R., 2018. CSIRO Australia Coastal Sealevel Simulations. v1. CSIRO. Data Collection. p. https://doi.org/10.4225/08/5a7280a3a0d2a.

Egbert, G. D. & Erofeeva, S. Y., 2002. Efficient inverse modeling of barotropic ocean tides. *J. Atmos. and Ocean. Tech.,* Volume 19, p. 183–204.

Erikson, L. et al., 2022. Global ocean wave fields show consistent regional trends between 1980 and 2014 in a multi-product ensemble. *Comms. Earth & Env.,* Volume 3, p. 320.

Feng, J. et al., 2018. Storm surge variation along the coast of the Bohai Sea. *Scientific Reports,* 8(1), pp. 1-10.

Ghanavati, M. et al., 2023. An assessment of whether long-term global changes in waves and storm surges have impacted global coastlines. *Scientific Reports,* Volume 13, p. 11549.

Harley, M. D. et al., 2017. Extreme coastal erosion enhanced by anomalous extratropical storm wave direction. *Sci. Rep.,* Volume 7, p. 6033.

Harley, M., Turner, I., Short, A. & Ranasinghe, R., 2011. A re-evaluation of coastal embayment rotation: The dominance of cross-shore versus alongshore sediment transport processes, Collaroy-Narrabeen Beach, southeast Australia. *Jnl. Geophys. Res. (Earth Surface),* Volume 116.

Hemer, M., 2010. Historical trends in Southern Ocean storminess: Long-term variability of extreme wave heights at Cape Sorell, Tasmania. *Geophys. Res. Lett.,* Volume 37, p. L18601.

Hemer, M. et al., 2013. Projected changes in wave climate from a multi-model ensemble. *Nature Clim. Change,* Volume 3, pp. 471-476.

Hersbach, H. et al., 2020. The ERA5 global reanalysis. *Q. J. R. Meteorol. Soc.,* Volume 146, pp. 1999-2049..

Hinkel, J. et al., 2013. A global analysis of erosion of sandy beaches and sea-level rise: An application of DIVA. *Global and Planetary Change,* Volume 111, pp. 150-158.

Hochet, A. et al., 2021. Sea state decadal variability in the North Atlantic: a review. *Climate,* Volume 9, p. 173.

Kim, D. Y. et al., 2017. Sea Level Rise and Storm Surge around the Southeastern Coast of Korea.. *Journal of Coastal Research,* 79(10079), pp. 239-243.

Komar, P., 1998. *Beach Processes and Sedimentation.* 544pp ed. s.l.:Prentice Hall.

Konlechner, T. et al., 2020. Mapping spatial variability in shoreline change hotspots from satellite data; a case study in southeast Australia. *Estuarine, Coastal and Shelf Science,* Volume 246, p. 107018.

Leach, C. et al., 2023. Measuring drivers of shoreline and subaerial beach change using limited datasets in a temperate, wave-dominated sandy system: Inverloch, Australia. *Ocean Coastal Managment,* Volume 240, p. 106641.

Liu, J. et al., 2022. The wave climate of Bass Strait and south-east Australia. *Ocean Modelling,* Volume 172, p. 101980.

Liu, J. et al., 2023. A high-resolution wave energy assessment of south-east Australia based on a 40-year hindcast. *Renewable Energy,* Volume 215, p. 118943.

Liu, J., Meucci, A. & Young, I., 2022. Projected wave climate of Bass Strait and south-east Australia by the end of the twenty-first century. *Climate Dynamics,* pp. 10.1007/s00382-022-06310-4.

Liu, J., Meucci, A. & Young, I., 2023. Projected 21st Century Wind-Wave Climate of Bass Strait and South-East Australia: Comparison of EC-Earth3 and ACCESS-CM2 Climate Model Forcing. *Jnl. Geophys. Res.,* Volume 128, p. e2022JC018996.

Liu, Q., Babanin, A., Rogers, E. & Zieger, S., 2021. Forty years of global wave hindcasts using the observation-based source terms: validation and geophysical applications. *Journal of Advances in Modeling Earth Systems,* 13(8).

Luijendijk, A. et al., 2018. The state of the world's beaches. *Scientific Reports,* Volume 8, pp. 1-11.

Masselink, G. et al., 2016. Extreme wave activity during 2013/2014 winter and morphological impacts along the Atlantic coast of Europe. *Geophy. Res. Lett.,* Volume 43, p. 2135–2143.

Meucci, A., Young, I., Hemer, M. K. E. & Ranasinghe, R., 2020. Projected 21st century changes in extreme wind-wave events. *Science Advances,* 6(24), p. eaaz7295.

Meucci, A. et al., 2023. 140 Years of Global Ocean Wind-Wave Climate Derived from CMIP6 ACCESS-CM2 and EC-Earth3 GCMs: Global Trends, Regional Changes, and Future Projections. *Jnl. Climate,* Volume 36, pp. 1605-1631.

Meucci, A. et al., 2023. Evaluation of spectral wave model physics as applied to a 100-year Southern Hemisphere extra tropical-cyclone sea state. *J. Geophys. Res. Oceans,* Volume 128, p. e2022JC018996.

Morim, J. et al., 2022. A global ensemble of ocean wave climate statistics from contemporary wave reanalysis and hindcasts. *Scientific Data,* Volume 9, p. 358.

Morim, J. et al., 2023. Understanding uncertainties in contemporary and future extreme wave events for broad-scale impact and adaptation planning. *Science Advances,* Volume 9, p. eade3170.

Muis, S. et al., 2016. A global reanalysis of storm surges and extreme sea levels. *Nat. Commun.,* Volume 7, p. 11969.

Nerem, R. et al., 2018. Climate-change–driven accelerated sea-level rise detected in the altimeter era. *Proc. National Academy of Sciences,* Volume 115, p. 2022–2025.

Paprotny, D., 2014. Trends in storm surge probability of occurrence along the Polish Baltic Sea coast.. *arXiv preprint arXiv.*

Ranasinghe, R., 2016. Assessing climate change impacts on open sandy coasts: A review. *Earth-Science Reviews,* Volume 160, pp. 320-332.

Ranasinghe, R., R., M., A., S. & G., S., 2004. The Southern Oscillation Index, Wave Climate, and Beach Rotation. *Marine Geology,* pp. 273-287.

Ranasinghe, R. et al., 2021. Climate change information for regional impact and for risk assessment. . In: *Climate Change 2021: The Physical Science Basis. Contribution of Working Group 1 to the Sixth Assessment Report of the Intergovernmental Panel on Climate Change.* Cambridge: Cambridge University Press, pp. 1767-1926.

Reguero, B. G., Losada, I. J. & Méndez., F. J., 2019. A recent increase in global wave power as a consequence of oceanic warming.. *Nature communications,* pp. 1-14.

Saha, S. et al., 2010. The NCEP Climate Forecast System Reanalysis. *B. Am. Meteorol. Soc.,* Volume 91, p. 1015–1057.

Sen, P., 1968. Estimates of the regression coefficient based on Kendals TAU. *Amer. Stats. Assoc. Journal,* pp. 1379-1389.

Shchepetkin, A. F. & McWilliams, J. C., 2005. The regional oceanic modeling system (ROMS): a split-explicit, free-surface, topography-following-coordinate oceanic model. *Ocean Modeling,* Volume 9, p. 347–404.

Takbash, A. & Young, I., 2020. Long-term and seasonal trends in global wave height extremes derived from ERA-5 reanalysis data. *J. Mar. Sci. & Eng.,* Volume 8, p. 1015.

Timmermans, B., Gommenginger, C., Dodet, G. & Bidlot, J.-R., 2020. Global Wave Height Trends and Variability from New Multimission Satellite Altimeter Products, Reanalyses, and Wave Buoys. *Geophys. Res. Lett.,* Volume 47, p. e2019GL086880..

Vitousek, S. et al., 2023. A model integrating satellite-derived shoreline observations for predicting fine-scale shoreline response to waves and sea-level rise across large coastal regions. *Jnl. Geophys. Res. Earth Surface,* p. e2022JF006936.

Vos, K., Harley, M., Turner, I. & Splinter, K., 2023. Pacific shoreline erosion and accretion patterns controlled by El Niño/Southern Oscillation. *Nature Geoscience,* Volume 16, p. 140–146.

Vousdoukas, M. et al., 2020. Economic motivation for raising coastal flood defenses in Europe. *Nature Comms.,* Volume 11, p. 2119.

Wang, X. L. & Swail, V. R., 2001. Changes of extreme wave heights in northern hemisphere oceans and related atmospheric circulation regimes. *J. Clim.,* pp. 2204-2221.

Wang, X. L. et al., 2009. Detection of external influence on trends of atmospheric storminess and northern oceans wave heights.. *Clim. Dyn. ,* pp. 189-203.

Watson, C. et al., 2015. Unabated global mean sea-level rise over the satellite altimeter era. *Nature Climate Change,* Volume 5, p. 565–568.

Young, I. & Ribal, A., 2019. Multi-platform evaluation of global trends in wind speed and wave height. *Science,* Volume 364, pp. 548-552.

Young, I. & Ribal, A., 2022. Can multi-mission altimeter datasets accurately measure long-term trends in wave height. *Rem. Sens.,* Volume 14, p. 974.

578 Young, I., Zieger, S. & Babanin, A., 2011. Global trends in wind speed and wave height.
579 *Science,* Volume 332, pp. 451-455.

580 Zheng, C. W. & Li, C. Y., 2017. Analysis of temporal and spatial characteristics of waves in the
581 Indian Ocean based on ERA-40 wave reanalysis,. *Applied Ocean Research,* Volume 63, pp. 217-
582 228.

583

584

585

586

587 **Tables and Figures**

588

| Coastal Segment | Recession (-0.05 to -1m/yr ) | Progradation (+0.05 to +1m/yr) | Stable (-0.05 to +0.05m/yr) |
|---|---|---|---|
| (a) 138°-140° | 40% | 45% | 15% |
| (b) 140°-142° | 40% | 46% | 14% |
| (c) 142°-144° | 53% | 27% | 20% |
| (d) 144°-146° | 37% | 49% | 14% |
| (e) 146°-148° | 40% | 50% | 10% |
| (f) 148°-150° | 60% | 30% | 10% |

589

590 Table 1: Percentage of coastal locations, as defined by the Bishop-Taylor, et al. (2021) dataset
591 receding (-0.05 to -1.00m/year), prograding (+0.05 to +1.00m/year) or stable ( ± 0.05m/year)
592 over the period 1988 to 2013.

593


Figure 1: The coastal region of south-east Australia comprising the study area. For analysis purposes the region is divided into six sections: (a) 138°-140°, (b) 140°-142°, (c) 142°-144°, (d) 144°-146°, (e) 146°-148° and (f) 148°-150° from west to east. The island of Tasmania is to the south of this coastline. (© Google Maps)

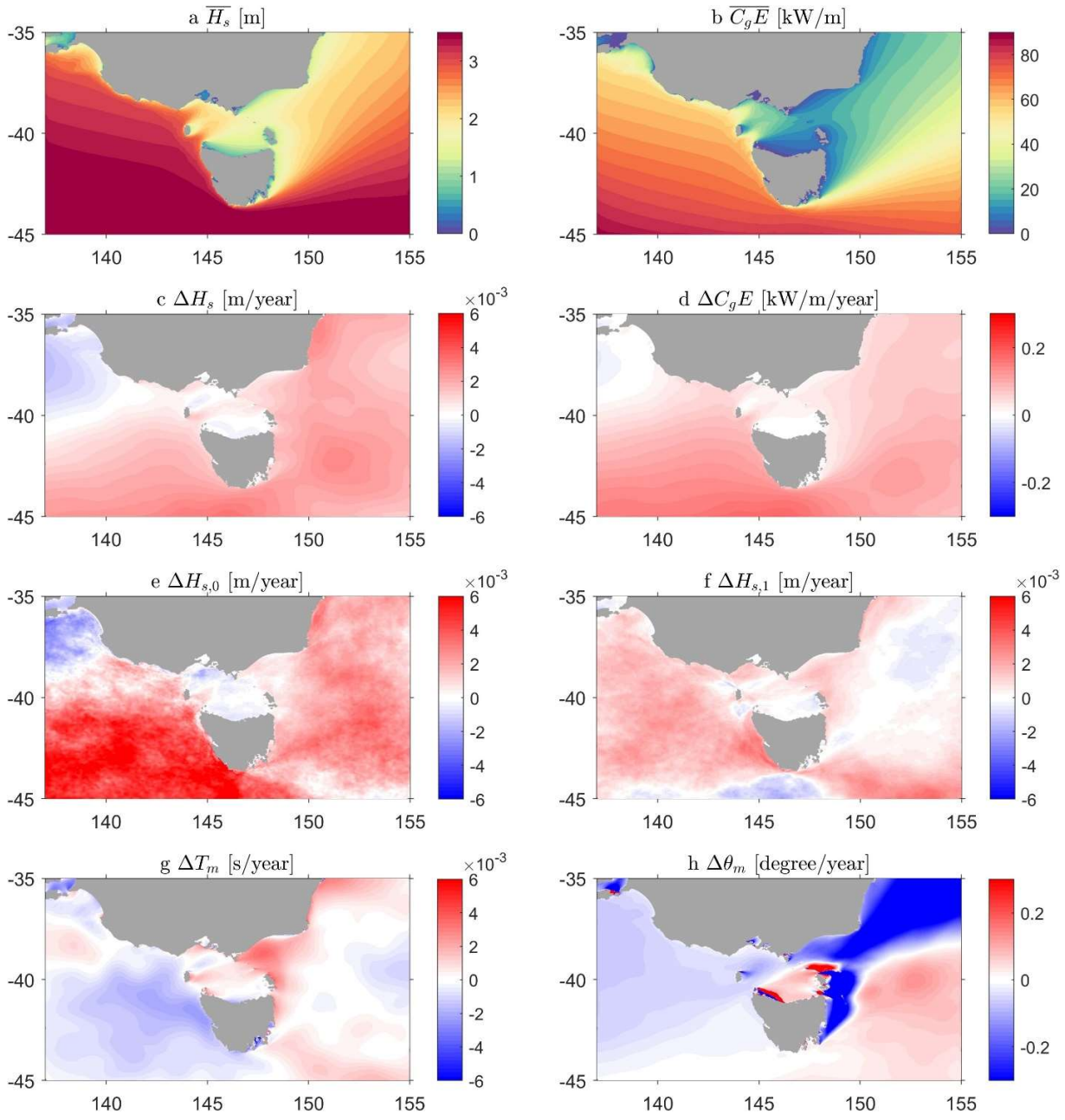


Figure 2: Wave climate and trends in the study region of south-eastern Australia over the period 1988 to 2013 as modelled by the Liu, et al. (2022) regional wave model. (a) mean significant wave height, (b) mean wave energy flux, (c) trend in significant wave height, (d) trend in wave energy flux, (e) trend in wind-wave portion of the spectrum, (f) trend in swell portion of the spectrum, (g) trend in mean wave period, (h) trend in mean wave direction.

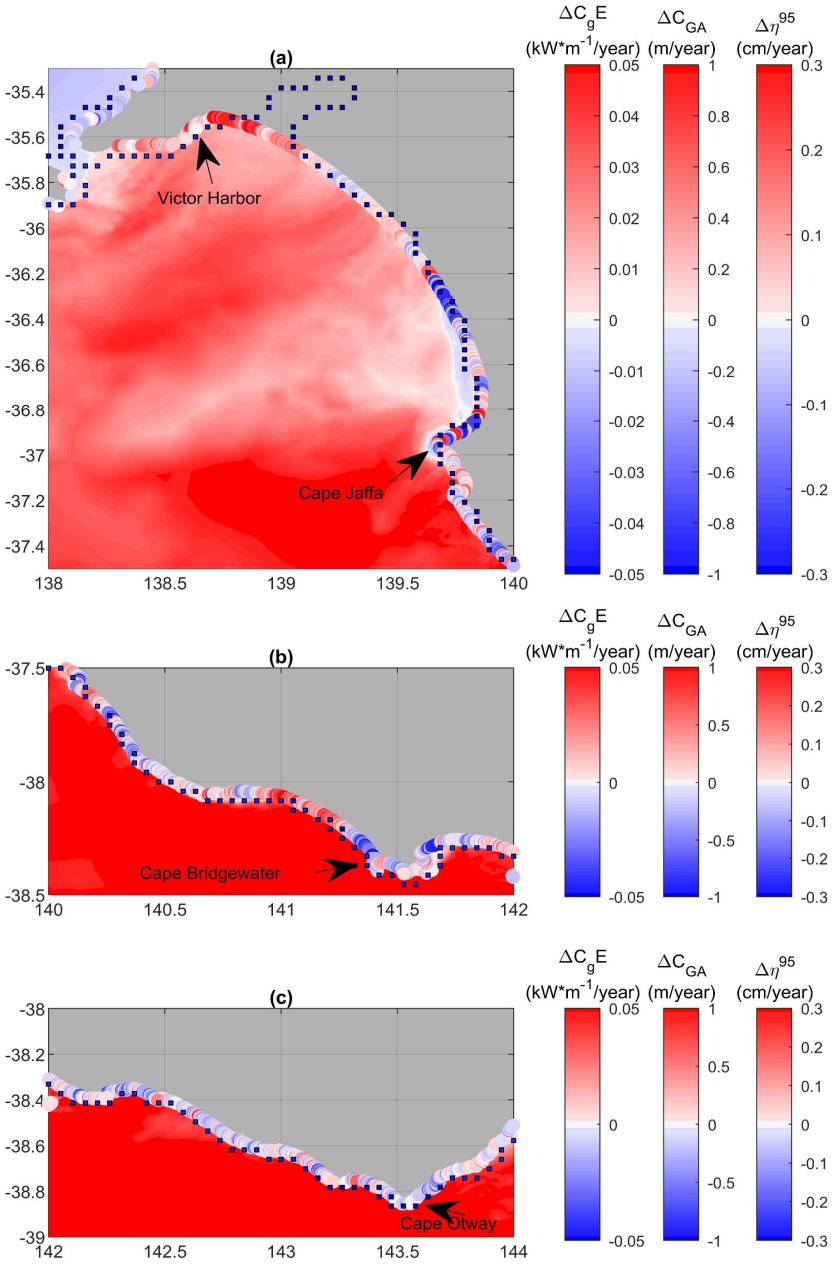


606

607 Figure 3 a-c: Trends in: wave energy flux, $\Delta C_g E$ shown as colour shaded values over the
608 domain, storm surge, $\Delta \eta^{95}$ shown as colour shaded squares at coastal model locations and
609 shoreline progradation/recession, $\Delta C_{GA}$ shown as colour shaded circles at beach locations.
610 Results shown for sections (a) 138E°-140E°, (b) 140E°-142E°, (c) 142E°-144E°.

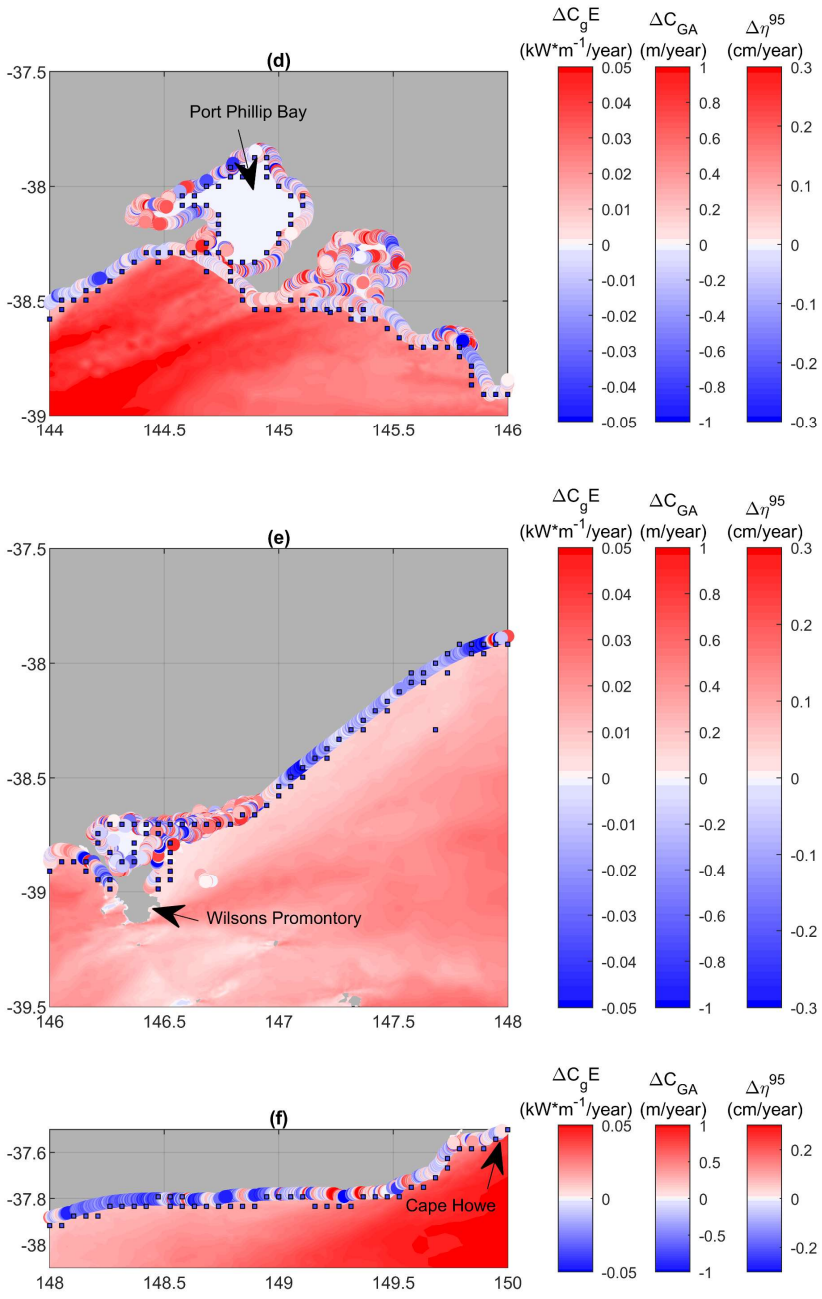


Figure 3 d-f: Trends in: wave energy flux, $\Delta C_g E$ shown as colour shaded values over the domain, storm surge, $\Delta \eta^{95}$ shown as a colour shaded squares at coastal model locations and shoreline progradation/recession, $\Delta C_{GA}$ shown as colour shaded circles at beach locations. Results shown for sections (d) 144E°-146E°, (e) 146E°-148E° and (f) 148E°-150E°.

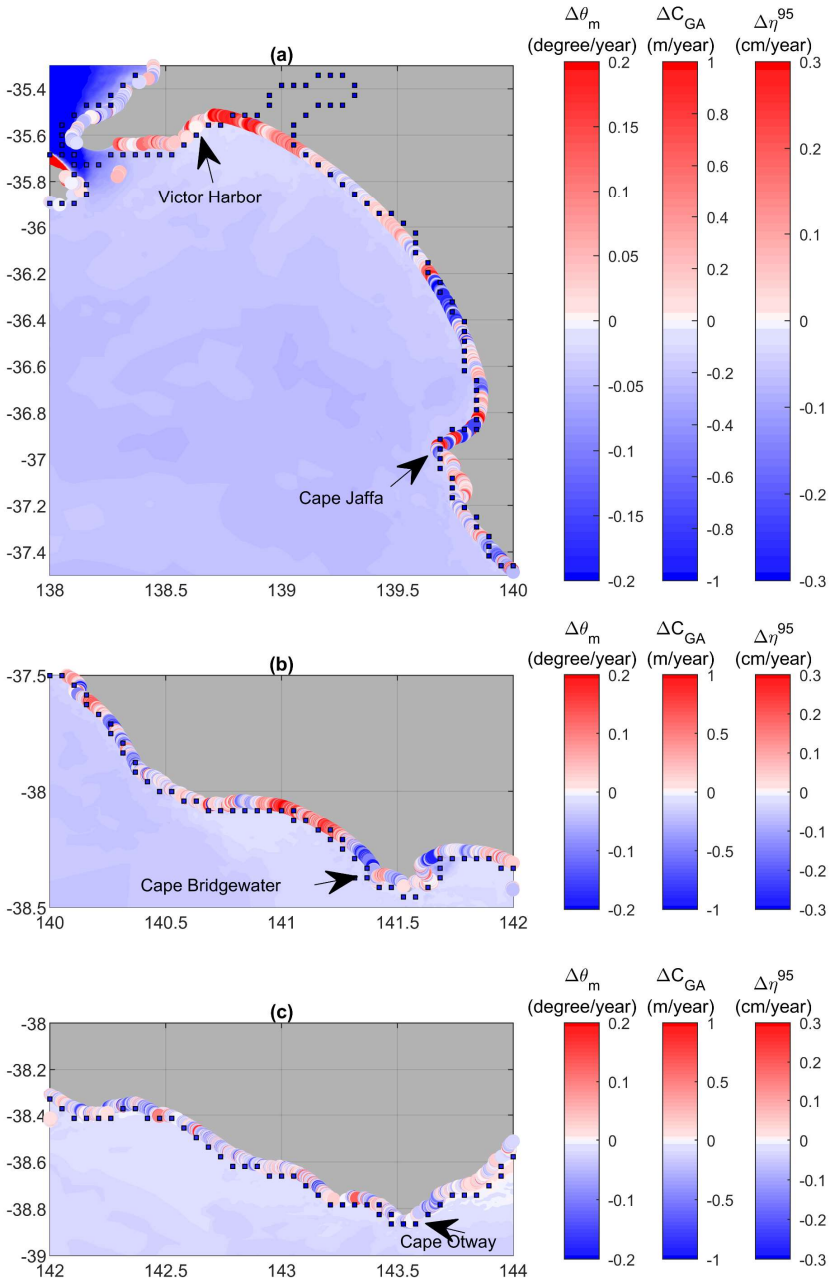


Figure 4 a-c: Trends in: mean wave direction, $\Delta\theta_m$ shown as colour shaded values over the domain, storm surge, $\Delta\eta^{95}$ shown as colour shaded squares at coastal model locations and shoreline progradation/recession, $\Delta C_{GA}$ shown as colour shaded circles at beach locations. Results shown for sections (a) 138E°-140E°, (b) 140E°-142E°, (c) 142E°-144E°.

635

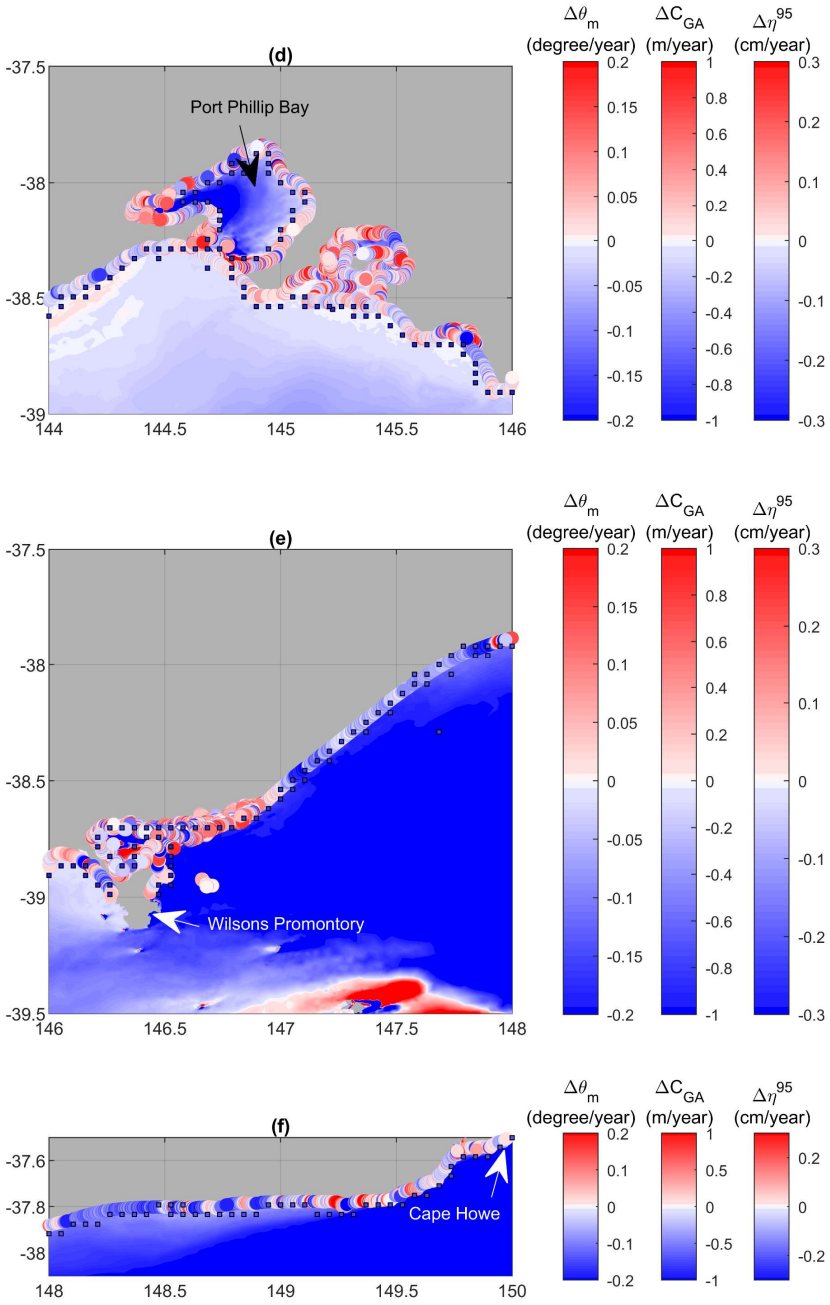


636 Figure 4 d-f: Trends in mean wave direction, $\Delta\theta_m$ shown as colour shaded values over the
637 domain, storm surge, $\Delta\eta^{95}$ shown as a colour shaded squares at coastal model locations and
638 shoreline progradation/recession, $\Delta C_{GA}$ shown as colour shaded circles at beach locations.
639 Results shown for sections (d) 144E°-146E°, (e) 146E°-148E° and (f) 148E°-150E°.

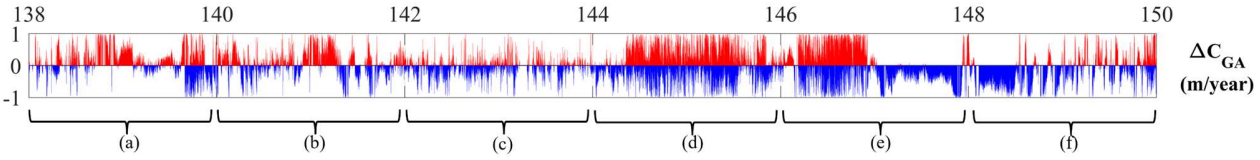


640 Figure 5: Bar chart showing values of progradation (red) and recession (blue), $\Delta C_{GA}$ at each
641 coastal location of the Bishop-Taylor, et al. (2021) dataset. Values are shown as a function of the
642 longitude (horizonal axis) and units are m/year. The regions shown in Figure 1 are labelled (a) to
643 (f).

644

645

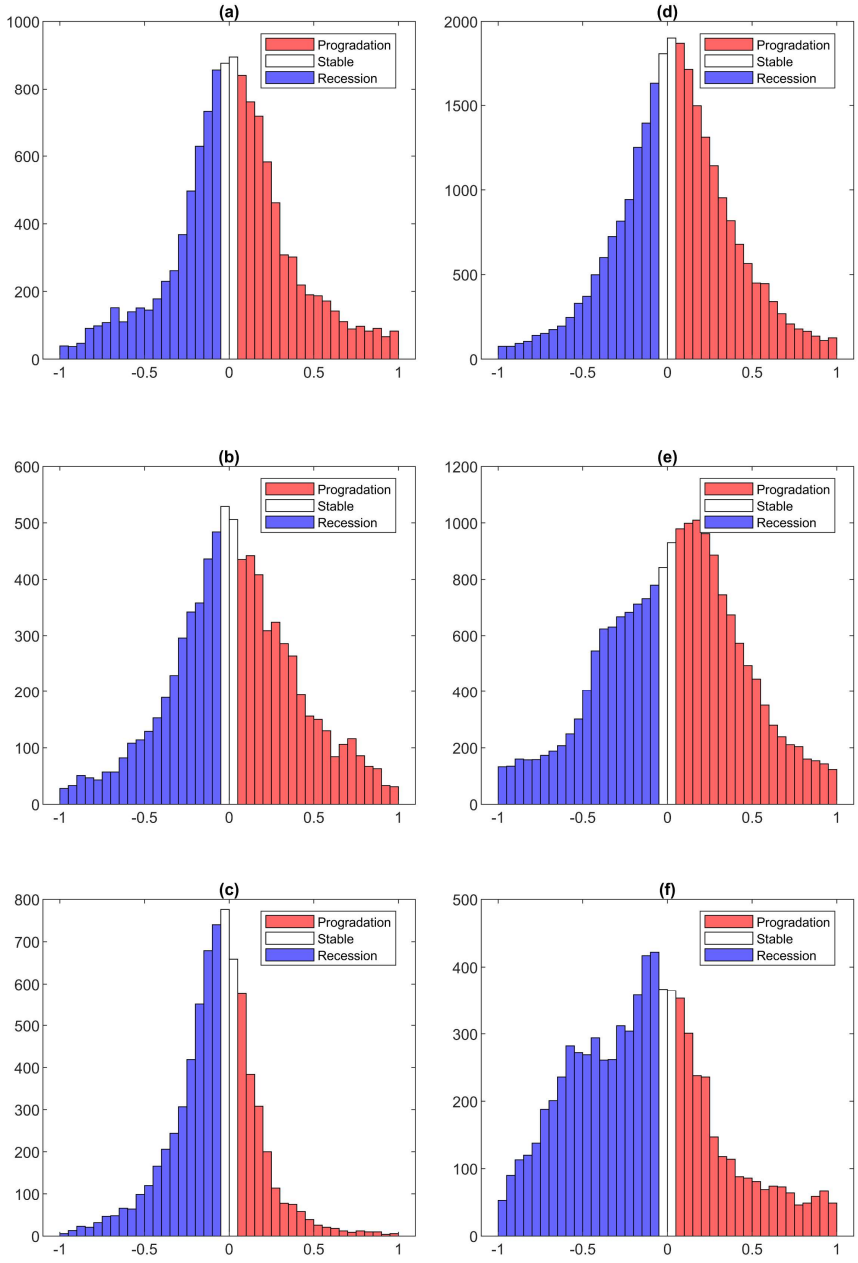


Figure 6: Histograms of progradation/recession rates for each of the coastal sections over the period 1988 to 2013. (a) 138E°-140E°, (b) 140E°-142E°, (c) 142E°-144E°, (d) 144E°-146E°, (e) 146E°-148E° and (f) 148E°-150E° from west to east.